JOURNAL OF MATERIALS SCIENCE 27 (1992) 2012–2018

Crystallization behaviour of Ni–Co-base metallic glasses by isochronal and isothermal annealing

W. ZHENG*†, D. W. KIRK‡, S. J. THORPE*
*Department of Metallurgy and Materials Science and ‡Department of Chemical Engineering, University of Toronto, 200 College St., Toronto, Ontario, Canada M5S 1A4

The crystallization behaviour of three amorphous alloys, $Co_{50}Ni_{25}Si_{15}B_{10}$, $Ni_{50}Co_{25}Si_{15}B_{10}$ and $Ni_{50}Co_{25}P_{15}B_{10}$, was studied by means of differential thermal analysis in conjunction with scanning transmission electron microscopy. Isochronal annealing showed a strong dependence of crystallization on scan rate over the range of 1.99 to 20.70 K min^{-1}. At high Co/Ni ratios, a sequential two-stage crystallization process involving primary MS-I phase followed by MS-II phase precipitation was observed. At low Co/Ni ratios MS-I and MS-II crystallization were concurrent and inseparable. Replacement of the metalloid Si with P as the glass-former dramatically reduced the activation energy for crystallization as well as the crystallization temperature. A mechanistic understanding of these findings was pursued in light of TEM/STEM microanalysis

1. Introduction

The thermal stability of metallic glasses is defined by the crystallization temperature, the mode of crystallization, the number of quenched-in nuclei, the activation energy for diffusion and the driving force for crystallization, i.e. the difference in free energy between the amorphous and possible crystalline phases. Differential scanning calorimetry (DSC) and differential thermal analysis (DTA) are useful in determining the crystallization temperature and heat of crystallization of phase changes occurring in metallic glasses. Peaks in a DTA plot corresponding to endothermic or exothermic crystallization in metallic glasses are not well defined and exhibit a finite temperature range over which the crystallization rate is a strong function of temperature. Crystallization temperatures are then defined as either the onset temperature, T_x, or the peak temperature, T_p. Activation energies for crystallization have thus been determined by plots of $\log\beta$ versus $1/T_x$ [1] or by $\log(T_x^2/\beta)$ versus $1/T_x$ [2] where β is the heating rate.

Since DTA techniques are isochronal in nature, complementary isothermal heat treatments are necessary to accurately define the kinetics of such transformations. Furthermore, DTA and isothermal annealing are indirect techniques and a direct correlation between the discontinuity in a physical property and the structure should be defined by X-ray or electron diffraction techniques.

The crystallization kinetics of many transition metal–metalloid glasses have been studied by many authors. However, alloys containing Co and Ni in the absence of Fe have received relatively little attention. Masumoto *et al.* [3] have previously studied the crystallization sequence in ternary Ni–Si–B and Co–Si–B metallic glasses and found for equivalent metalloid contents that Co-base glasses are more stable than Ni-base glasses. Crystallization in the ternary glasses proceeded by a two-stage MS-I, MS-II crystallization sequence. Inoue and co-workers [4, 5], in later studies, also investigated the crystallization of quaternary (Fe, Ni, Co)$_{78}Si_{10}B_{12}$ alloys. They found that the stability decreased in the order Fe, Co, Ni. Crystallization occurred by one of three mechanisms based on metalloid concentration via MS-I and MS-II phase transformations. In (Ni, Co)$_{78}Si_{10}B_{12}$ two exothermic peaks were observed independent of the Ni:Co ratio. Very few data are available on the heat of crystallization and crystallization temperatures and activation energies for MS-I and MS-II phases.

The purpose of this study was to determine the phase distribution, the activation energy of crystallization, crystallization enthalpies and temperatures of $Co_{50}Ni_{25}Si_{15}B_{10}$, $Ni_{50}Co_{25}Si_{15}B_{10}$ and $Ni_{50}Co_{25}P_{15}B_{10}$ by DTA and isothermal heat treatments and to characterize the structure and composition of the crystalline phases by transmission and scanning transmission electron microscopy (TEM/STEM). These results were then used to ensure the stability of these materials for use as potential electrocatalysts in fuel cells and electrolysers [6, 7] in which they are used at elevated temperatures.

2. Experimental procedure

Little characterization of the electrocatalytic activity of metallic glasses has been performed. Ni–Co-base metallic glasses were selected to investigate the kinetics of hydrogen evolution in aqueous alkaline environments. The glasses were fabricated from Co chunks

† *Present address*: IREQ, Institut de recherche d'Hydro-Québec, 1800 Montée Ste-Julie, Varennes (Québec), Canada J3X ISI.

0022–2461

($\geqslant$ 99.9%), Ni powder (99.9%), NiB powder (99%) and either Si chunks (99.99%) or Ni_2P powder (99.5%). The materials, combined in the appropriate ratios, were pre-melted in a quartz tube in an induction furnace to form an ingot prior to melt-spinning. Ribbons 4 mm wide by 40 μm thick were produced by single-roller melt-spinning. The details of the spinning process are given elsewhere [7]. The exact compositions of the metallic glasses were determined by inductively coupled plasma (ICP) analysis and are summarized in Table I. Initial structural characterization of each glass was performed by X-ray diffraction using 40 kV FeK_α radiation with an Mn filter at a scan rate of 0.5° min^{-1}. All the alloys displayed broad spectral profiles as shown in Fig. 1, characteristic of amorphous materials and indicative of a small degree of retained crystallinity.

TABLE I Composition of amorphous alloys

Nominal formula	ICP results (at %)				
	Ni	Co	Si	P	B
$Co_{50}Ni_{25}Si_{15}B_{10}$	29	48	12	–	11
$Ni_{50}Co_{25}Si_{15}B_{10}$	53	24	13	–	10
$Ni_{50}Co_{25}P_{15}B_{10}$	49	26	–	15	10

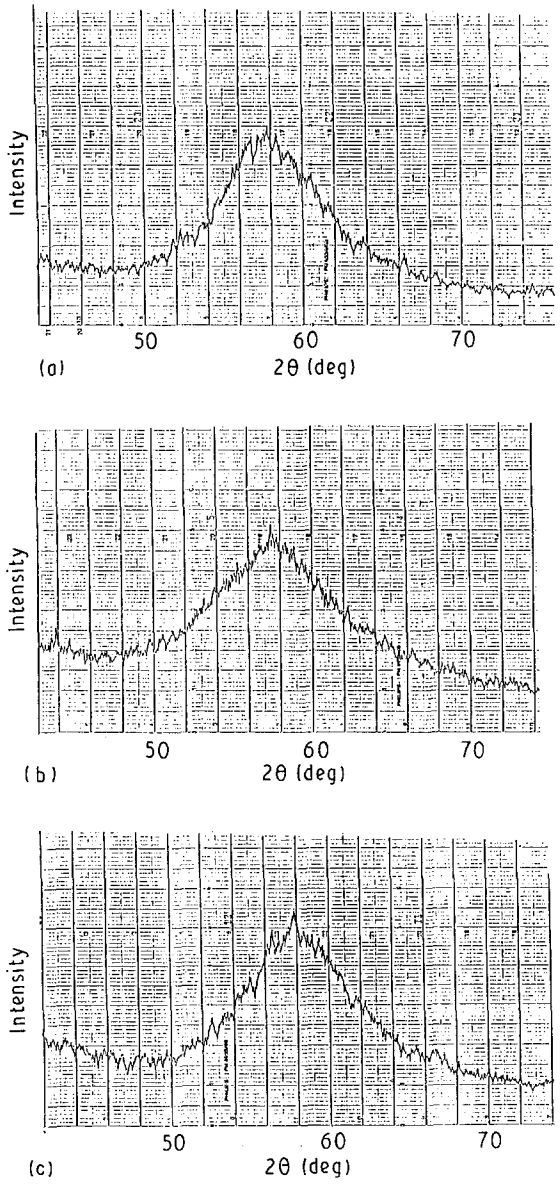

Figure 1 X-ray diffraction patterns of amorphous alloys: (a) $Co_{50}Ni_{25}Si_{15}B_{10}$, (b) $Ni_{50}Co_{25}Si_{15}B_{10}$ and (c) $Ni_{50}Co_{25}P_{15}B_{10}$.

2.1. Differential thermal analysis

A Premco Model P50 was used to determine the dynamic crystallization temperature and enthalpy of crystallization of each alloy. The differential thermal analyser was calibrated against the melting endotherms of 99.999 wt % Sn, 99.999 wt % Pb and 99.99 wt % Zn for each heating rate utilized. Calibration curves for actual versus experimental temperature and enthalpy per unit area traced were determined as a function of heating rate. The reference material consisted of powdered δ-Al_2O_3.

Small fragments of each alloy totalling 20 mg in weight were cut from the as-received ribbon and placed in intimate contact in an aluminium crucible. The chamber was then purged for 1 h at a flow rate of 0.472 l min^{-1} with high-purity argon. Some tests were also performed on 40 mg samples to improve the accuracy of the transformation enthalpy determinations. Heating rates of 1.99, 4.3, 10.9 and 20.70 K min^{-1} were used and all scans terminated at 823 K. Crystallization temperatures determined by this method were used to define subsequent isothermal annealing cycles.

2.2. Isothermal heat treatment

Rectangular sections approximately 4 mm × 10 mm × 40 μm were cut from the as-received ribbon for the devitrification studies. All samples were sealed in evacuated quartz capsules. Prior to sealing, each capsule was evacuated and back-filled with ultra-high purity argon a minimum of three times to limit the amount of oxidation upon heat treatment.

Samples of each glass were heat-treated to produce a high-temperature multiphase (MP) transformation. Temperature selection was based on the DTA results of this study. Annealing was performed in a 45% $NaNO_3$ + 55% KNO_3 salt bath using a Lindberg Model 56622 furnace. Temperature stability and distribution were determined to be better than ± 3 K.

2.3. TEM/STEM analysis

Scanning transmission electron microscopy is the preferred technique to ensure complete amorphousness in the as-received ribbon, since low volume fractions of crystallites are not adequately resolved by X-ray diffraction [8]. Discs 3 mm in diameter for TEM were punched from the as-received ribbon and heat-treated. Final preparation involved jet-polishing on a Struers Tenupol in either (a) 7:1 ethanol:60% perchloric acid or (b) a mixture of 5% perchloric + 10% nitric in ethanol. Optimum thinning conditions were as follows: for electrolyte (a), voltage 6–10 V at 20 °C; and for electrolyte (b), 30–40 V at − 15 °C with a flow-rate setting of 2 (Tenupol). All samples were examined on a Hitachi H-800 TEM/STEM equipped with a Kevex X-ray detector and

microdiffraction unit. The minimum diffraction spot size was 10.0 nm.

3. Results

3.1. Differential thermal analysis

The results of the DTA experiments on $Co_{50}Ni_{25}Si_{15}B_{10}$, $Ni_{50}Co_{25}Si_{15}B_{10}$ and $Ni_{50}Co_{25}P_{15}B_{10}$ as a function of heating rate are summarized in Tables II to IV, respectively. In $Co_{50}Ni_{25}Si_{15}B_{10}$, a two-stage sequential transformation of MS-I and MS-II was observed independent of heating rate. However, in $Ni_{50}Co_{25}Si_{15}B_{10}$ and $Ni_{50}Co_{25}P_{15}B_{10}$ a single transformation was observed corresponding to the concurrent transformation of MS-I and MS-II phases for all heating rates. No separation of the two transformations was possible. Increasing the heating rate produced an increase in the observed transformation temperatures for all stages of crystallization. Temperature corrections for heating rate from the calibration procedure were applied and the corrected values reported.

Activation energies for crystallization were determined by Ozawa plots of $\log\beta$ versus $1/T$ [1] for each transformation as shown in Figs 2 to 4 for $Co_{50}Ni_{25}Si_{15}B_{10}$, $Ni_{50}Co_{25}Si_{15}B_{10}$ and $Ni_{50}Co_{25}P_{15}B_{10}$, respectively. Activation energies were also determined by Kissinger plots of $\ln(T^2/\beta)$ versus $1/T$ [2], where β is the heating rate and T is the peak temperature, as shown in Figs 5–7 for $Co_{50}Ni_{25}Si_{15}B_{10}$, $Ni_{50}Co_{25}Si_{15}B_{10}$ and $Ni_{50}Co_{25}P_{15}B_{10}$, respectively. Enthalpies of crystallization also increased with heating rate even after an enthalpy correction for heating rate from the calibration procedure. Ozawa plots revealed activation energies for MS-I and MS-II crystallization of 459 and 696 kJ mol^{-1}, respectively, for $Co_{50}Ni_{25}Si_{15}B_{10}$. Kissinger plots for the same transformations in $Co_{50}Ni_{25}Si_{15}B_{10}$ yielded similar activation energies of 471 and 718 kJ mol^{-1} for MS-I and MS-II transformations, respectively. In $Ni_{50}Co_{25}Si_{15}B_{10}$ the combined activation energies for MS-I + MS-II were 781 and 808 kJ mol^{-1} as determined by Ozawa and Kissinger plots, respectively. $Ni_{50}Co_{25}P_{15}B_{10}$ displayed activation energies of 411 (Ozawa) and 421 kJ mol^{-1} (Kissinger).

3.2. TEM/STEM analysis

Transmission electron microscopy was used as a screening criterion for crystallization in each glass as a function of surface finish and heat treatment. Any evidence of crystallites in the ribbon resulted in rejection of that ribbon in further testing. For the samples selected, no crystallites were visible in all foils thinned from the as-received ribbon. Diffraction analysis of all these materials revealed only a diffuse ring pattern as shown in Fig. 8. Crystallization of the glass by a high-

TABLE III Crystallization parameters as a function of heating rate for $Ni_{50}Co_{25}Si_{15}B_{10}$[a]

Heating rate (K min^{-1})	T_g (K)	T_1 (K)	H_1 (J g^{-1})
1.99	–	760 ± 1	55.2 ± 4.8
4.30	–	765 ± 3	64.0 ± 5.7
10.90	730	770 ± 4	64.8 ± 2.9
20.70	–	774 ± 1	–

[a] T_1: peak transformation temperatures for MS-I and MS-II; H_1: enthalpies of transformation for MS-I and MS-II. Data based on at least three trials for each scan rate.

TABLE IV Crystallization parameters as a function of heating rate for $Ni_{50}Co_{25}P_{15}B_{10}$[a]

Heating rate (K min^{-1})	T_g (K)	T_1 (K)	H_1 (J g^{-1})
1.99	608 ± 2	673 ± 1	39.3 ± 3.5
4.30	620 ± 1	680 ± 3	44.7 ± 4.2
10.90	628 ± 4	689 ± 4	50.1 ± 3.4
20.70	–	694 ± 1	–

[a] T_1: peak transformation temperatures for MS-I and MS-II; H_1: enthalpies of transformation for MS-I and MS-II. Data based on at least three trials for each scan rate.

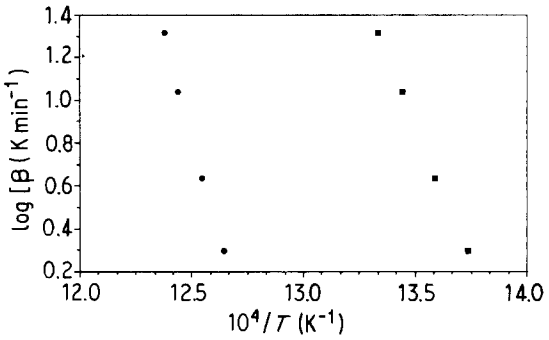

Figure 2 Ozawa plot of $\log\beta$ versus $1/T$ for $Co_{50}Ni_{25}Si_{15}B_{10}$. Activation energies for (■) crystallization of MS-I, $E = 459$ kJ mol^{-1}; (●) crystallization of MS-II, $E = 696$ kJ mol^{-1}.

TABLE II Crystallization parameters as a function of heating rate for $Co_{50}Ni_{25}Si_{15}B_{10}$[a]

Heating rate (K min^{-1})	T_g (K)	T_1 (K)	T_2 (K)	H_1 (J g^{-1})	H_2 (J g^{-1})
1.99	638 ± 3	728 ± 5	791 ± 2	13.2 ± 1.5	16.1 ± 2.1
4.30	653 ± 15	751 ± 20	797 ± 4	14.6 ± 0.3	44.0 ± 3.6
10.90	686 ± 2	744 ± 2	804 ± 3	14.9 ± 1.7	33.2 ± 3.8
20.70	680 ± 4	750 ± 3	808 ± 1	–	–

[a] T_1, T_2: peak transformation temperatures for MS-I and MS-II, respectively; H_1, H_2: enthalpies of transformation for MS-I and MS-II, respectively. Data based on at least three trials for each scan rate.

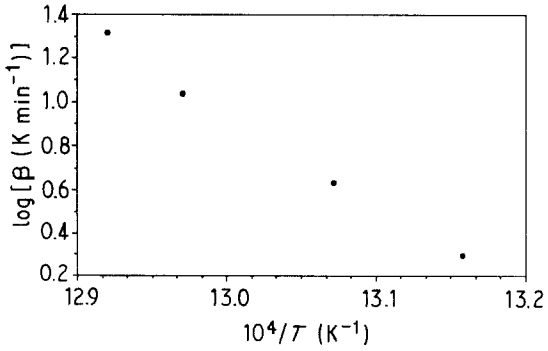

Figure 3 Ozawa plot of $\log\beta$ versus $1/T$ for $Ni_{50}Co_{25}Si_{15}B_{10}$. Activation energy for crystallization of MS-I + MS-II, $E = 781$ kJ mol^{-1}.

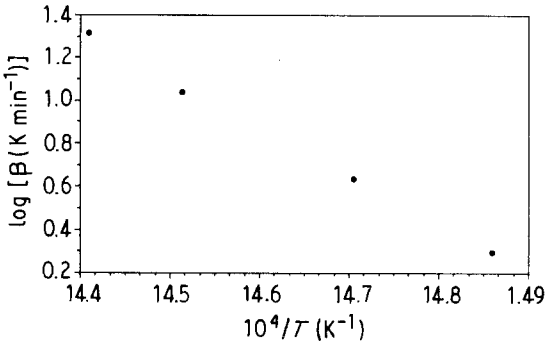

Figure 4 Ozawa plot of $\log\beta$ versus $1/T$ for $Ni_{50}Co_{25}P_{15}B_{10}$. Activation energy for crystallization of MS-I + MS-II, $E = 411$ kJ mol^{-1}.

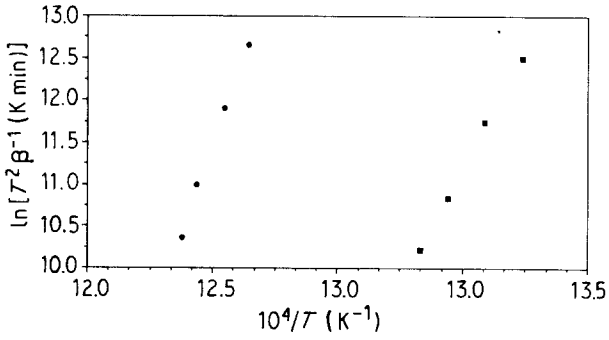

Figure 5 Kissinger plot of $\ln(T^2/\beta)$ versus $1/T$ for $Co_{50}Ni_{25}Si_{15}B_{10}$. Activation energies for (■) crystallization of MS-I, $E = 471$ kJ mol^{-1}; (●) crystallization of MS-II, $E = 718$ kJ mol^{-1}.

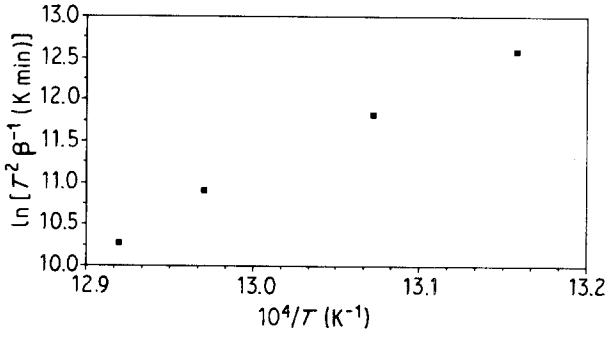

Figure 6 Kissinger plot of $\ln(T^2/\beta)$ versus $1/T$ for $Ni_{50}Co_{25}Si_{15}B_{10}$. Activation energy for crystallization of MS-I + MS-II, $E = 808$ kJ mol^{-1}.

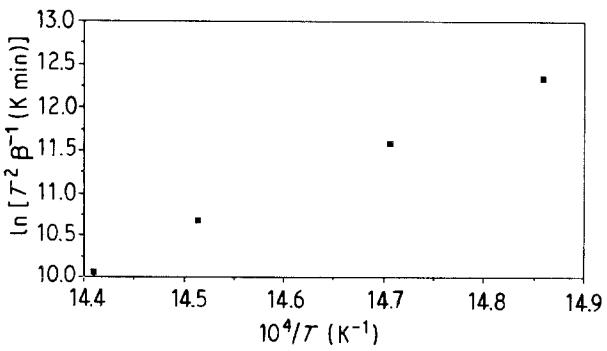

Figure 7 Kissinger plot of $\ln(T^2/\beta)$ versus $1/T$ for $Ni_{50}Co_{25}P_{15}B_{10}$. Activation energy for crystallization of MS-I + MS-II, $E = 421$ kJ mol^{-1}.

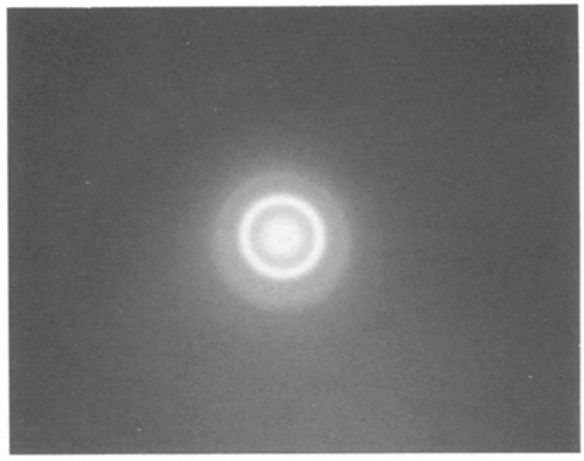

Figure 8 Diffraction pattern showing diffuse haloes characteristic of an amorphous material for as-received $Co_{50}Ni_{25}Si_{15}B_{10}$.

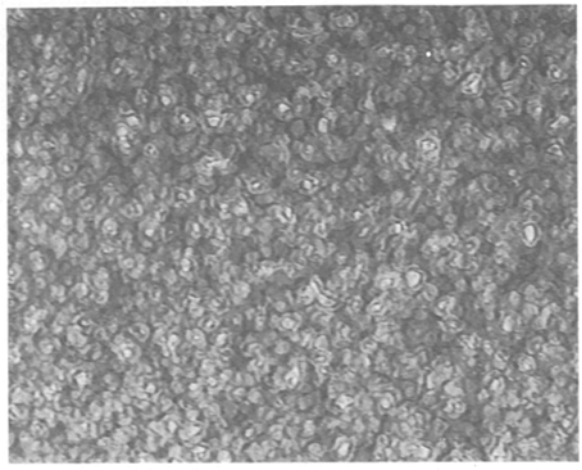

Figure 9 Transmission electron micrograph of $Co_{50}Ni_{25}Si_{15}B_{10}$ showing MS-I and MS-II phases. (Magnification 20 000 ×)

temperature, short-term anneal (MP anneal) produced strong partitioning of the glass into an (Ni, Co) solid solution (MS-I) phase and a series of MS-II phases. The fine distribution of MS-I and MS-II phases ranged from 3 to 200 nm in size as illustrated in Fig. 9 for $Co_{50}Ni_{25}Si_{15}B_{10}$. TEM/STEM analyses of the fine distribution of phases are summarized in Table V.

TABLE V Electron diffraction data for Co–Ni–(Si, P)–B glasses

Alloy	Phase	Crystal structure	Lattice parameters (nm)		
			This work	Other work	Reference
$Co_{50}Ni_{25}Si_{15}B_{10}$	MS-I	h.c.p.	$a = 2.48$ $c = 4.02$	$a = 2.51$ $c = 4.07$	[4]
	(Co, Ni)B	Orthorhombic	$a = 3.81$ $b = 6.68$ $c = 3.00$		
$Ni_{50}Co_{25}Si_{15}B_{10}$	MS-I	f.c.c.	$a = 3.32$	$a = 3.52$	[4]
	(Co, Ni)B	Orthorhombic	$a = 3.21$ $b = 6.97$ $c = 3.01$		
	$(Co, Ni)_3Si$	Cu_3Au	$a = 3.47$		
$Ni_{50}Co_{25}P_{15}B_{10}$	MS-I	f.c.c.	$a = 3.581$	–	–
	$(Ni, Co)_3P$	Tetragonal	$a = 0.896$ $c = 0.443$	$a = 0.895$ $c = 0.439$	[11]

4. Discussion

4.1. DTA and crystallization

The number of stages of crystallization observed for $Co_{50}Ni_{25}Si_{15}B_{10}$ in Table II as a function of heating rate is in good agreement with that observed by Inoue *et al.* [4] for $Co_{52}Ni_{26}Si_{10}B_{12}$. The latter authors observed an MS-I transformation temperature of 657 K and an MS-II transformation temperature of 793 K at a scan rate of 5 K min^{-1}. Si is more effective than B in raising the transformation temperature of Ni–Co metallic glasses. By comparison with this study, transformation temperatures for MS-I and MS-II were determined to be 751 and 797 K, respectively. The higher Si:B ratio in $Co_{50}Ni_{25}Si_{15}B_{10}$ would increase both the transformation temperatures although this would be offset by the slightly different Co:Ni ratio. An increase in the metalloid content would also slightly delay the MS-I transformation to higher temperatures.

Only a single-stage crystallization process was observed for the $Ni_{50}Co_{25}Si_{15}B_{10}$ metallic glass as seen in Table III. An increase in the Ni:Co ratio at constant metalloid content decreased the transformation temperature and altered the mechanism from a two-stage to a single-stage crystallization process. This is in contrast to a two-stage crystallization process observed by Inoue *et al.* [4] for $Ni_{52}Co_{26}Si_{10}B_{12}$. The latter authors observed an MS-I transformation temperature of 639 K and an MS-II transformation temperature of 773 K at a scan rate of 5 K min^{-1} compared with a single transformation temperature of 765 K for $Ni_{50}Co_{25}Si_{15}B_{10}$ in this work. The slight increase in metalloid content seems unlikely to have delayed the MS-I transformation to the point where it is concurrent with the MS-II transformation.

A single-stage crystallization process was also observed for the $Ni_{50}Co_{25}P_{15}B_{10}$ metallic glass, providing further evidence that the crystallization sequence is highly dependent on the Ni:Co ratio. At constant Ni:Co ratio, the replacement of Si with P decreased the transformation temperature. This is in agreement with previous work [9] on Fe-base metallic glasses.

A kinetic analysis of the reaction rates for the various crystallization stages can also be performed by DTA to determine the activation energies and order of reactions. Kissinger [2] originally postulated, for reactions of the type solid → solid + gas, that the peak temperature varies with the heating rate according to the equation

$$\frac{\ln(T^2/\beta)}{1/T} = \frac{E}{R} \tag{1}$$

where β is the heating rate, T is the peak temperature, E is the activation energy and R is the gas constant. In the derivation of Equation 1, Kissinger assumed that the rate of heat evolution is proportional to the rate of the reaction and that the peak differential deflection occurs when the reaction rate is a maximum. In the detailed derivation of Equation 1, the activation energy can be determined for a simple decomposition reaction regardless of the reaction order.

Ozawa [1] also proposed that the heating rate of a reaction varies with the temperature for a *first-order* reaction according to the equation

$$\log\beta = -0.4567\left(\frac{\Delta E}{RT}\right) - 2.315 + \log\left(\frac{A\Delta E}{R}\right) - \log G(x) \tag{2}$$

where ΔE is the activation energy of crystallization, A is the frequency factor and $G(x)$ is a function of the extent of conversion and time. Contrary to Kissinger, in the derivation of Equation 2, Ozawa did not assume that the observed height of the temperature difference from the baseline (rate of heat evolution) was proportional to the rate of the process. Kissinger assumed that this height was proportional to the rate of the process according to the temperature dependence on time, position of the temperature measurement and the rate of conversion. Ozawa found that the temperature was a function of the extent of conversion, rate of conversion, the time and position by considering the heat flow in and out of the sample and the presence of a temperature differential within the sample.

A comparison of the activation energies determined by the two methods is given by a comparison of Figs 2 and 5 for $Co_{50}Ni_{25}Si_{15}B_{10}$, Figs 3 and 6

for $Ni_{50}Co_{25}Si_{15}B_{10}$, and Figs 4 and 7 for $Ni_{50}Co_{25}P_{15}B_{10}$. Activation energies determined by the Kissinger method for the crystallization of MS-I and MS-II are 471 and 718 kJ mol^{-1}, respectively, for $Co_{50}Ni_{25}Si_{15}B_{10}$. By assuming that the reaction order is unity, the activation energies determined by the method of Ozawa are determined as 459 and 696 kJ mol^{-1}, respectively, for the crystallization of MS-I and MS-II. The measured activation energy for MS-I and MS-II crystallization is lower with the method of Ozawa than with that of Kissinger although the differences are minor. The good agreement observed between the two methods indicates that the reaction order is close to unity. Similar results were obtained for the $Co_{50}Ni_{25}Si_{15}B_{10}$ and $Co_{50}Ni_{25}Si_{15}B_{10}$ alloys.

The activation energies observed for MS-I transformation in $Co_{50}Ni_{25}Si_{15}B_{10}$ were much higher than that observed in Metglass 2826A [10]. This transformation is sensitive not only to the amount and type of metalloids present, but the nature of the major metallic species. If the as-received glass contained a large concentration of pre-existing nuclei for MS-I crystallization, this would lower the activation energy for this step alone, since the nucleation and growth of MS-II has been observed [10] to occur only at the MS-I–amorphous interphase boundary after partitioning and diffusion of the metalloid elements in the amorphous matrix. However, careful TEM/STEM analysis of the as-received ribbon revealed no discernible evidence of crystallinity unless the size of such nuclei was below the resolution of this technique (< 1.0 nm), which is unlikely.

The heat of fusion as a function of temperature for pure Sn, Pb, and Zn was used to calibrate the enthalpy per unit area (E/A) under the peak of the curve for the determination of enthalpies of crystallization of each glass as reported in Tables II to IV. Similar correction factors were obtained for scan rates of 1.99, 4.30 and 10.90 K min^{-1} but a large shift in the E/A ratio was observed for a scan rate of 20.70 K min^{-1}. Generally, the heat of fusion increased with increasing scan rate. A comparison of the enthalpy of $Co_{50}Ni_{25}Si_{15}B_{10}$ and $Ni_{50}Co_{25}Si_{15}B_{10}$ reveals that the sums of the transformation enthalpies are nearly equivalent, although the transformation sequence is different. A replacement of Si with P lowered the transformation enthalpy.

4.2. TEM/STEM analysis

Using the transformation temperatures determined above, TEM/STEM analysis was performed on samples after isochronal annealing and after 60 min anneals at 823 K. No evidence of crystallinity was observed in as-received ribbon by TEM/STEM analysis, and only a weak diffuse halo identical to that observed in the as-received glass was observed as shown in Fig. 8.

Considering the transformation temperatures determined by DTA analysis in Tables II–IV, annealing all of the as-received glasses at a temperature of 823 K for 60 min (MP anneal) should promote crystallization of the glass by a two-stage process of MS-I and MS-II crystallization in agreement with the TTT diagrams for the ternary systems Fe–Si–B and Co–Si–B obtained by Masumoto *et al.* [3]. MS-I phases in each of the systems were composed primarily of the major metallic element of the glass and reflected the crystal structure of that element; Ni-rich glasses had face-centred cubic (f.c.c.) MS-I phases and Co-rich glasses had a mixture of hexagonally closed-packed (h.c.p. phases) and f.c.c. phases. A summary of the diffraction analysis is given in Table V. This is in good agreement with the observations of Inoue *et al.* [4] for quaternary Ni–Co–Si–B alloys, with slight shifts in lattice parameters accountable by changes in the solubility between the major metallic species.

Analysis of the MS-II phases proved more difficult due to the greater variation in composition. A good fit with diffraction analysis was obtained for the phases orthorhombic (Co, Ni)B, Cu_3Au–Ni_3Si, and tetragonal $(Co, Ni)_3P$. Inoue *et al.* [4] also noted in ternary alloys the presence of orthorhombic Co_3B and Ni_3B. Orthorhombic phases of the type $(Ni, Co)_3B$ were observed although an accurate determination of a consistent lattice spacing proved difficult. More work is required to standardize many of the MS-II phases observed. Slight shifts in the observed lattice spacings compared to the actual lattice spacings in Table V are easily accounted for by the mutual solubility of Ni and Co in these compounds and the interchange of metalloid species.

5. Conclusions

Crystallization of $Co_{50}Ni_{25}Si_{15}B_{10}$ by isochronal annealing showed that devitrification occurred by a two-stage crystallization process into MS-I and MS-II phases, independent of scan rate. The MS-I phase displayed an h.c.p. crystal structure and occurred at transformation temperatures of 728 to 750 K over scan rates of 1.99 to 20.70 K min^{-1} and possessed an activation energy of transformation of 465 $\pm$ 6 kJ mol^{-1} and enthalpy of 14 $\pm$ 1 J g^{-1}. Complex MS-II phases were observed over a transformation temperature range of 791 to 797 K with an activation energy of transformation of 706 $\pm$ 12 kJ mol^{-1}.

Varying the Ni:Co ratio at constant metalloid concentration (alloy $Ni_{50}Co_{25}Si_{15}B_{10}$) altered the crystallization sequence to a single stage, concurrent MS-I and MS-II transformations with a reduction in the transformation temperatures to 760 to 774 K over scan rates of 1.99 to 20.70 K min^{-1} with an activation energy of transformation of 794 $\pm$ 18 kJ mol^{-1}.

Substitution of silicon by phosphorus (alloy $Ni_{50}Co_{25}P_{15}B_{10}$) did not alter the crystallization sequence from a single-stage transformation, although the activation energy for transformation decreased significantly to 416 $\pm$ 5 kJ mol^{-1} at a transformation temperature of 673 to 694 K over scan rates of 1.99 to 20.70 K min^{-1}.

Good agreement was obtained with the kinetic theories of Ozawa and Kissinger and the reaction order for transformation in all the alloys was near unity.

Acknowledgements

The authors would like to acknowledge the financial support of NSERC, Canmet Energy Mines and Resources, Nickel Development Institute and the University Research Incentive Fund. The authors are indebted to W. Johnson and K. Kwong for their help in performing the DTA analysis.

References

1. T. OZAWA, *J. Therm. Anal.* **2** (1970) 301.
2. H. E. KISSINGER, *Anal. Chem.* **29** (1957) 1702.
3. T. MASUMOTO, Y. WASEDA, H. KIMURA and A. INOUE, *Sci. Rep. Res. Inst. Tohoku Univ.* **26A** (1976) 21.
4. A. INOUE, T. MASUMOTO, M. KIKUCHI and T. MINEMURA, *ibid.* **27A** (1979) 127.
5. A. INOUE, T. MASUMOTO and M. KIMURA, *ibid.* **27A** (1979) 159.
6. K. LIAN, D. W. KIRK and S. J. THORPE, *Electrochim. Acta.* **36** (1991) 537–545.
7. K. LIAN, MASc thesis, University of Toronto (1990).
8. S. J. THORPE, G. PALUMBO and K. T. AUST, in "Mechanical Behavior of Rapidly Solidified Materials", edited by S. M. L. Sastry and B. A. MacDonald (AIME, New York, 1986) p. 59.
9. M. NAKA, S. TOMIZAWA, T. WATANABE and T. MASUMOTO, in Proceedings of 2nd International Conference on Rapidly Quenched Metals (MIT Press, Boston, 1976) p. 273.
10. S. J. THORPE, B. RAMASWAMI and K. T. AUST, *Acta Metall.* **36** (1988) 795.
11. H. CHANG and S. SASTRI, *Metall. Trans.* **8A** (1977) 1063.

Received 24 April 1990
and accepted 15 January 1991